INTERNATIONAL ATOMIC ENERGY AGENCY
UNITED NATIONS EDUCATIONAL, SCIENTIFIC AND CULTURAL ORGANIZATION

INTERNATIONAL CENTRE FOR THEORETICAL PHYSICS
34100 TRIESTE (ITALY) - P.O.B. 586 - MIRAMARE - STRADA COSTIERA 11 - TELEPHONE: 2240-1
CABLE: CENTRATOM - TELEX 460892-I

SMR/208 - 27

SPRING COLLEGE IN MATERIALS SCIENCE

ON

"METALLIC MATERIALS"

(11 May - 19 June 1987)

NEUTRON AND X-RAY SCATTERING FROM METALLIC ALLOYS, EXAFS (Part III)

C.H. DE NOVION
SESI
Centre d'Etudes Nucléaires
B.P. No. 6
92260 Fontenay-aux-Roses
France

i)

SPRING COLLEGE IN MATERIALS SCIENCE
ON
"METALLIC MATERIALS"
(11 May – 19 June 1987)

NEUTRON AND X-RAY SCATTERING FROM METALLIC ALLOYS, EXAFS.

Part III : ELASTIC DIFFUSE AND SMALL-ANGLE SCATTERING

C.H. de NOVION
Section d'Etude des Solides Irradiés
Centre d'Etudes Nucléaires
B.P. 6, F-92260 Fontenay-aux-Roses
France

III ELASTIC DIFFUSE AND SMALL-ANGLE SCATTERING

III.1. Introduction

In a real crystal, one may encounter two types of static disorder :
- a composition disorder (atoms of different nature),
- a position disorder (the atoms are not at the exact average crystal sites).

If the elastic scattering of X-rays and neutrons by a perfect crystal gives Bragg reflexions only, static disorder brings a weak diffuse intensity between the Bragg peaks (as was shown first by GUINIER [1] and COWLEY [2]). The analysis of this diffuse intensity allows in principle to deduce :
- atomic pair correlations,
- static atomic displacements relative to the crystal sites (due to size effect, for example).

We are here interested by elastic diffuse scattering (scattered and incident particle have the same energy), which is from an static disorder (On the other hand, inelastic diffuse scattering can occur : it is due to dynamic effects, such as pre-transitional "soft mode" in organic one-dimensional conductors for example [3]).

Schematically, one can separe several types of behaviours :
- If the ordered alloy displays only composition disorder, the elastic diffuse scattering is periodic in the reciprocal space, and is the Fourier transform of the composition fluctuations in the real crystal. In particular, if the components A and B (of scattering lengths b_A and b_B) of an alloy $A_{1-x}B_x$ are randomly distributed, the diffuse scattering cross-section for N atoms is the same value : $d\sigma/d\Omega = Nx(1-x)(b_A - b_B)^2$, constant in the reciprocal space. If there is a tendency to segregation, $d\sigma/d\Omega$ will show maxima in $\vec{Q} = 0$ (small angle scattering, see § III.6) and at the Bragg peaks. If there is tendency to order A and B, $d\sigma/d\Omega$ will show

maxima between the Bragg peaks, corresponding in general to superstructure peaks at lower temperatures.

- If the alloy is dilute ($x \ll 1$) with only non-interacting B solutes, the diffuse intensity, which is <u>not</u> periodic in the reciprocal space, will give the Fourier transform of the atomic displacement field in the crystal, due to a B atom (if the displacements are weak). $d\sigma/d\Omega$ diverges at the Bragg peaks (Huang scattering)
- If the alloy shows altogether short-range ordering and position disorder, techniques have been developed to separate the two contributions if the displacements are not too important (see § III. 5).

Diffuse scattering can be observed in electron diffraction patterns from a transmission electron microscope: this allows (rapid) local qualitative studies (such as short-range order in a precipitate, for example); but the intensity distribution cannot be interpreted quantitatively.

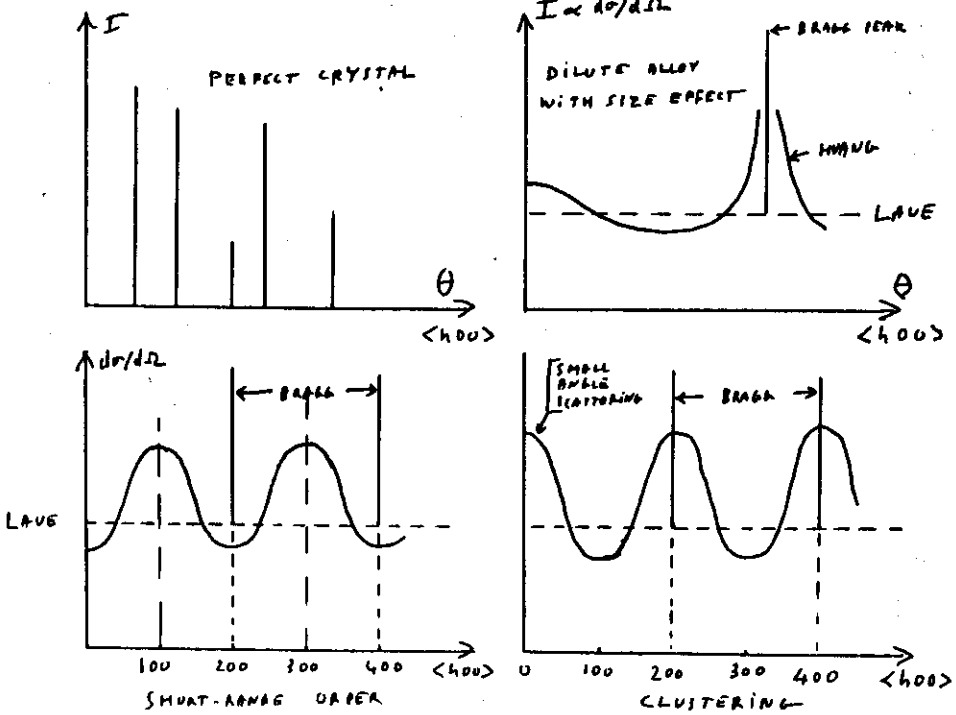

III. 2 Experimental

X-ray and neutron diffuse scattering measurements are difficult, because one has to extract a weak signal from an important background. The experiments need to be done on single crystals in order, to be correctly interpreted, and are long. But the theory is rather well advanced and straightforward.

(a) X-ray diffuse scattering far from the Bragg peaks

One has to correct for many contributions: Compton scattering (by calculation), thermal diffuse scattering (by measurements at several temperatures and extrapolation to 0 K), fluorescence, air scattering by the sample and harmonic $\lambda/2$ of the monochromator (by the use of a solid-state detector).

The main contributions measured by the detector are shown on the figure → for irradiated Al, at 4 K, containing $5 \cdot 10^{-4}$ Frenkel pairs [4]

Samples are typically 1 cm² × 1 mm. The flux has to be monitored, and a focussing monochromator before the sample is necessary.

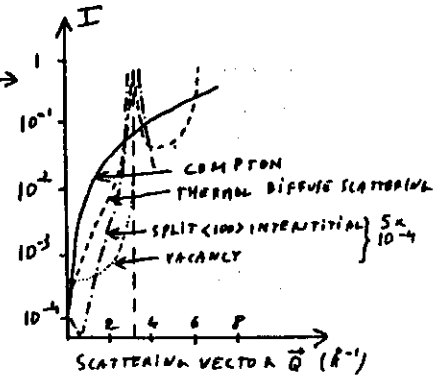

The reader will find description of two apparatus in ref [5] (for short-range order studies) and [6] (for radiation induced point-defect studies).

(b) X-ray diffuse scattering near the Bragg peaks

Huang scattering, which gives the long-range strain field of defects, is much larger than diffuse scattering far from the Bragg peaks; but it needs high resolution ($\Delta h = 10^{-3}$ in the reciprocal space), which may be obtained at the expense of intensity, for example with a monochromator of small mosaicity [7]

(c) Neutron diffuse scattering (far from the Bragg peaks)

- Inelastic scattering can be separated by time-of-flight technique or analyser crystal,
- Elastic incoherent scattering is nearly constant in the reciprocal space (it varies as the Debye-Waller factor) and has to be calculated; unfortunately, incoherent scattering cross-sections of many elements are not well known; that of hydrogen is very large; a chemical determination of the quantity of hydrogen impurities in the sample is not always available (a easy),
- Paramagnetic scattering in strongly paramagnetic samples can be calculated,
- For polycrystals, multiple (elastic) Bragg scattering has absolutely to be avoided, generally by using long wavelength (above the Bragg cut-off: $\lambda > 2d_{max}$).

Samples have to be large ($\sim 1\,cm^3$). Absolute values of $d\sigma/d\Omega$ are obtained using a vanadium standard. Experiments can be made with a 3-axis spectrometer (see figure 15, part I) or a two-axis + time-of-flight + multicounter spectrometer (see figure 6, part I).

In any case, the quality of the shielding is of main importance.

Typical values:

- Study of short-range order in Ni_3Fe on the 3 axis-4 circle D10 spectrometer (ILL, Grenoble) [8]: the exploration of the whole necessary volume for the study of $d\sigma/d\Omega$ by the 2nd order Sparks and Borie method needed about 2 weeks (1496 measuring points, 5' per point, 100 to 2000 counts per point (Laue $\equiv$ 200 counts), from which 20 for background, without sample, 20 for incoherent + paramagnetic).
- Study of the dilute alloy $NiO_{0.03c}$ on the 2 axis D7 (ILL, Grenoble) [9]: 2 days to explore the (001) reciprocal lattice plane (up to $|\vec{Q}| = 3\,\text{Å}^{-1}$) (32 detectors, 30' per point, 200 to 1300 counts per point (Laue $\equiv$ 500 counts), 100 counts for background, 30 counts for incoherent (in fact H impurities)).

III.3 Short-range order in alloys

(a) General formulation of the scattering cross-section.

Consider an $A_{1-x}B_x$ binary alloy, with no long-range order, no static displacements, containing N atoms, 1 atom per cell, defined by its position $\vec{R_i}$. The elastic cross-section is (see § I):

$$d\sigma/d\Omega\ (\vec{Q}) = \sum_{i,j}^{N} b_i b_j \exp i\vec{Q}(\vec{R_i} - \vec{R_j})$$

We introduce the occupation factors $c_i = \begin{cases} 1 & \text{if } i \text{ occupied by } B \\ 0 & \text{if } i \text{ occupied by } A \end{cases}$

and the Ising operator $\sigma_i = 2(c_i - x)$ ($2(1-x)$ for B, $-2x$ for A),

which represent the fluctuations of occupation around the average concentration

($\overline{c} = \frac{1}{N}\sum_i c_i = x$, $\overline{\sigma} = x\sigma_B + (1-x)\sigma_A = 0$, $\sigma_i = \pm 1$ for $A_{0.5}B_{0.5}$).

The scattering amplitude at site i is $b_i = \underbrace{\overline{b}}_{\text{average value}} + \underbrace{\frac{\sigma_i}{2}(b_B - b_A)}_{\text{fluctuation}}$

One can easily show that $\sum_{i,j} \sigma_i e^{i\vec{Q}(\vec{R_i} - \vec{R_j})} = 0$, and therefore that:

$$d\sigma/d\Omega\ (\vec{Q}) = \underbrace{\sum_{i,j}^{N} \overline{b}^2 e^{i\vec{Q}.(\vec{R_i} - \vec{R_j})}}_{\text{Bragg scattering } (\vec{Q} = \vec{\tau}_{hkl})} + \underbrace{\frac{(b_A - b_B)^2}{4} \sum_{i,j} \sigma_i \sigma_j e^{i\vec{Q}.(\vec{R_i} - \vec{R_j})}}_{\text{Diffuse scattering } \neq 0 \text{ if } \vec{Q} \neq \vec{\tau}_{hkl}}$$

For a crystal with a large number of sites, many pairs of atoms are distant by the same vector $\vec{R_i} - \vec{R_j}$, and for all these pairs we replace $\sigma_i\sigma_j$ by $\overline{\sigma_i \sigma_j}$. As there is no long-range order (LRO), the correlation between fluctuations of occupation of site i and j is equal to zero for sufficiently far neighbours, and practically all the atoms of the crystal will have the same number of neighbours participating to the scattering: $\overline{\sigma_i \sigma_j} = \overline{\sigma_0 \sigma_n}$.

The short-range order (SRO) elastic cross-section outside the Bragg peaks is therefore:

$$d\sigma/d\Omega)_{SRO}\ (\vec{Q}) = \frac{(b_A - b_B)^2}{4} \cdot N \sum_n \overline{\sigma_0 \sigma_n}\, e^{i\vec{Q}.\vec{R_n}}$$

Fourier transform of the composition fluctuation correlations.

If one introduces the Cowley-Warren SRO coefficients [2]:

$\alpha(\vec{R}_n) = 1 - p^B(\vec{R}_n)/x$ where $p_B(\vec{R}_n)$ is the probability to have an atom B distant of $\vec{R}_n$ from A situated at the origin,

$\alpha(\vec{R}_n) = 0$ for complete disorder, $\alpha(\vec{R}_n \to \infty) = 0$

$\alpha(\vec{R}_n) \begin{cases} <0 \\ >0 \end{cases}$ means $\begin{cases} \text{A-B pairs} \\ \text{A-A and B-B pairs} \end{cases}$ tend to place at distance $\vec{R}_n$

One can check easily that $\langle c_0 c_n \rangle = x^2 + x(1-x)\,\alpha(\vec{R}_n)$

$\langle \sigma_0 \sigma_n \rangle = x(1-x)\,\alpha(\vec{R}_n)$

Finally, taking into account that $\alpha(\vec{R}=0) = 1$, one has:

$$\left(\frac{d\sigma}{d\Omega}\right)_{SRO}(\vec{Q}) = N x(1-x)(b_A - b_B)^2 \left[1 + \sum_{n\neq 0} \alpha(\vec{R}_n)\, e^{i\vec{Q}\cdot\vec{R}_n}\right] \quad /1/$$

The short-range order elastic diffuse scattering cross-section is periodic in reciprocal space.

For complete disorder $\alpha(R \neq 0) = 0$ and one obtains the LAUE formula $d\sigma/d\Omega)_{SRO} = N x(1-x)(b_A - b_B)^2$ (constant).

For powders, $\left(\frac{d\sigma}{d\Omega}\right)_{SRO}(\vec{Q}) = N x(1-x)(b_A - b_B)^2 \left[1 + \sum_i n_i \alpha_i \frac{\sin(Q R_i)}{Q R_i}\right]$

where n_i is the number of atoms on the i-th neighbour shell.

(b) Interpretation in terms of the electronic structure

One knows (see the course by F. GAUTIER) that the internal energy of an alloy $A_{1-x}B_x$ can be approximately written for a given structure (fcc, bcc, ...):

$E = E_0 + E_{configuration}$,

where $E_0 \simeq$ a few eV, depends only on the average atomic volume; $E_{configuration}$ ($\simeq$ a few 10^{-1} eV) depends on the atomic distribution of A and B atoms.

In the Ising approximation, $E_{conf} = \frac{1}{4}\sum_{i,j\neq i} V(|\vec{R}_i - \vec{R}_j|)\,\sigma_i\sigma_j$,

where $V(|\vec{R}_i - \vec{R}_j|) = \frac{1}{2}\left[V_{AA}(|\vec{R}_i - \vec{R}_j|) + V_{BB}(|\vec{R}_i - \vec{R}_j|) - 2V_{AB}(|\vec{R}_i - \vec{R}_j|)\right]$,

V_{AA}, V_{BB} and V_{AB} being <u>effective</u> interatomic potentials taking

into account the screening by conduction electrons, and σ_i is the Ising operator defined in § III.3.@. $V(|\vec{R}_i - \vec{R}_j|)$ depends on the composition x.

With a mean-field approximation (where the energy of an atom A depends only on the <u>average</u> configuration of its near neighbour shells, neglecting fluctuations), KRIVOGLAZ [10] and CLAPP and MOSS [11] have shown a fundamental relation (KCM) between the Fourier transforms $\tilde{\alpha}(\vec{Q}) = \sum_{\vec{R}} \alpha(\vec{R})\, e^{-i\vec{Q}\cdot\vec{R}}$ and $\tilde{V}(\vec{Q}) = \sum_{\vec{R}} V(\vec{R})\, e^{-i\vec{Q}\cdot\vec{R}}$, with $\alpha(\vec{R}=0) = 1$ and $V(\vec{R}=0) = 0$, one has:

$$\tilde{\alpha}(\vec{Q})\ \left(\propto d\sigma/d\Omega)_{SRO}\right) = \frac{C}{1 + 2x(1-x)\,\tilde{V}(\vec{Q})/k_B T} \quad /2/$$

where C is a constant $= \Omega^* \left|\int \frac{d^3Q}{\alpha(\vec{Q})}\right|^{-1}$ (Ω^* = reciprocal lattice cell volume).

Relation /2/ shows that the maxima of diffuse scattering $\tilde{\alpha}(\vec{Q})$ coincide with the absolute minima of $\tilde{V}(\vec{Q})$, which occur for $\vec{Q} = \vec{Q}_m$.

When $T \to \infty$, $\tilde{\alpha}(\vec{Q}) \to 1$ and $\alpha(\vec{R}_{nm} \neq 0) \to 0$ ($d\sigma/d\Omega \to$ LAUE)

When cooling, $\tilde{\alpha}(\vec{Q}_m)$ increases, and the critical temperature T_c is defined as that for which $\tilde{\alpha}(\vec{Q}_m) = \infty$, i.e.

$k_B T_c = -2x(1-x)\,\tilde{V}(\vec{Q}_m)$ $\quad (\tilde{V}(\vec{Q}_m) < 0)$.

At $T = T_c$, one predicts a superstructure (or phase separation if $\vec{Q}_m = 0$), with superlattice Bragg reflexions in $\vec{Q}_m$, at the same positions as the diffuse scattering maxima. This is effectively the case for many systems (Cu_3Au, $Ti\,Co_{0.64}$, Ni_3Fe, ...). But the KCM approximation, which is a high temperature statistic approximation (analogous to the Curie-Weiss law for magnetic susceptibility), looses its validity near T_c which is not correctly predicted.

In some cases, such as Ni_4Mo, the superlattice reflexions do not coincide with the diffuse scattering maxima; this can be attributed for example:

- to geometrical reasons: for a given composition x, in the superstructure considered, each site must be occupied by A or B, but cannot have a fractional occupation;
- to lattice distortions which can occur with long-range ordering.

If the pair potentials are limited to near neighbours, one can draw diagrams in the space of coordinates $V_1, V_2, V_3, \ldots$ defining regions corresponding each to a given set of $\widetilde{\Phi}_n$ values [11]. This is shown below for V_1, V_2 and fcc or bcc alloys.

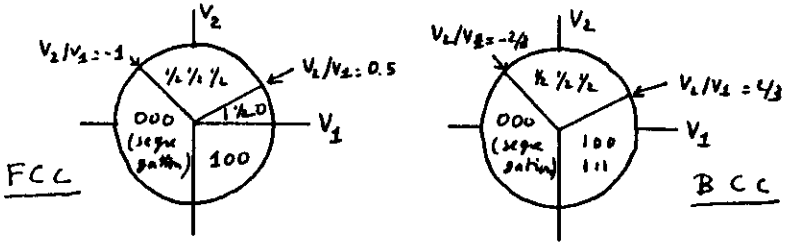

Recent experiments have allowed to obtain precise $\tilde{\varphi}(\vec{q})$ data and to show that $V(\vec{R})$ calculated from relation /2/ has the oscillatory form predicted theoretically for interacting ions pairs screened by a free electron gas (analogy with Friedel oscillations for impurities in metals).

$V(\vec{R})$ decreases more rapidly with distance in the case of transition metal alloys (Ni_3Fe) than in normal or noble metal alloys (Cu_3Au, see figure below).

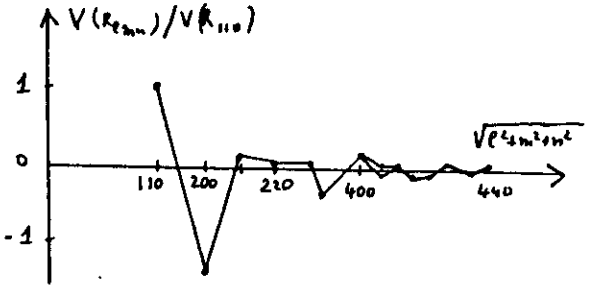

(Calculated from the KCM formula, from X-ray diffuse scattering data on Cu_3Au [12]).

Of course, the KCM formula /2/ does not give accurate potentials, especially if the measurements are made at $T < 1.5\,T_c$.

A more sophisticated formula, due to Tahir-Kheli [13], obtained by high temperature expansion of the free energy, is the following:

$$\tilde{\alpha}(\vec{q}) = \frac{C}{1 + 2x(1-x)\beta\,\tilde{V}(\vec{q}) - 2(1-2x)^2 x(1-x)\beta^2\left[N^{-1}\sum_{\vec{\tau}} V(\vec{\tau})\,V(\vec{q}-\vec{\tau})\right] + O(\beta^3)}$$

where $\beta = 1/k_B T$ and $\sum_{\vec{\tau}}$ is taken on all points $\vec{\tau}$ of the 1st Brillouin zone.

Recently, GILDER and VIGNESOULT [14] have calculated $\tilde{\alpha}(\vec{q})$ from precisely well known potentials for Li - 10% at. Mg at 473 K, using the Tahir-Kheli formula, and then the KCM potentials from $\tilde{\alpha}(\vec{q})$: the relative KCM potentials $V_{200}^{KCM}/V_{110}^{KCM}$, $V_{211}^{KCM}/V_{110}^{KCM}$, ... when large by 60% than the real values.

More fundamentally, on titanium nitride $TiN_{0.82}$ where short-range ordering of nitrogen vacancies occurs on the f.c.c. metalloid sublattice, (diffuse maxima in $\frac{1}{2}\frac{1}{2}\frac{1}{2}$), the (temperature independant) KCM potentials obtained from in-situ neutron scattering experiments at 700, 800 and 900 °C (see § III.5), are compared below to the potentials obtained by the Monte-Carlo (MC) method [15]; the 2nd order predicted critical temperatures are also given; the interatomic effective potential is shown to be very short-range, as V_1 and V_2 are much large than $V_3, V_4, \ldots$. The Monte-Carlo potentials are $\simeq 50\%$ higher than the KCM values, but the mean-field relation value V_2^{KCM}/V_1^{KCM}, V_3^{KCM}/V_1^{KCM}, V_4^{KCM}/V_1^{KCM}, are reasonably good, which is possibly due to the large $T/T_c \simeq 2$.

V_1 (meV)		V_2 (meV)		V_3 (meV)		V_4 (meV)		V_2/V_1		T_c (°C)	
KCM	MC	KCM	MC	KCM	MC	KCM	MC	KCM	MC	KCM	MC
56.2	81.7	39.8	60.6	1.2	2.5	2.4	3.8	0.71	0.74	250	350

$TiN_{0.82}$

The "Cluster-Variation Method" (CVM) due originally to KIKUCHI [16] is presently developed to calculate more precise potentials from diffuse scattering data; in this approximation, the alloy is described as an assembly of clusters, eventually overlapping, and containing n crystal sites each; each configuration i of the clusters

is characterized by an internal energy E_{int} ; in the f.c.c. lattice, the best approximation is obtained by taking the "quadruple tetrahedron - octahedron" cluster, which contains $n = 10$ atoms, and up to 4th neighbour pairs.

Another interpretation of diffuse scattering data has been directly in terms of imaging the Fermi surface shape: if the Fermi surface presents flat parallel parts distant by $2\vec{k_F}$, one will have a quasi- one dimensional behaviour in this direction, and a dielectric susceptibility of the electron gas which will present a sharp maximum at $2\vec{k_F}$: $\tilde{V}(\vec{Q})$ will be minimum and $\tilde{\chi}(\vec{Q})$ maximum at $\vec{Q} = 2\vec{k_F}$. This idea has been applied to Co/Pt alloys [17] and to $Ti_{0.85}O_{0.85}$ [18].

(c) Example

- Segregation in Cu - Ni alloys

VRIJEN and RADELAAR [19] have obtained the short-range order coefficients in $Cu_x Ni_{1-x}$ polycrystals by neutron diffuse scattering after quench from 400 - 700 °C. Using isotopic substitution, the alloy $^{65}Cu_{0.435}{}^{62}Ni_{0.565}$ presents a zero average scattering length $\overline{b}$ and therefore no simple or multiple Bragg scattering. This allows to use small wavelength neutrons and explore up to $|\vec{Q}| = 6\ Å^{-1}$. The increase of $d\sigma/d\Omega$ when $Q \to 0$ shows a tendency to segregation, confirmed by the numerical analysis : α_1 is large and positive (+0.12 at 406 °C) : a Cu has a probability equal to 0.503 to have a 1st neighbour Cu (instead of the random probability 0.435). From the temperature dependence of the diffuse scattering, the authors deduce a miscibility gap around 350 °C for $x = 0.435$, i.e. at a temperature where kinetics are too low to observe experimentally phase separation.

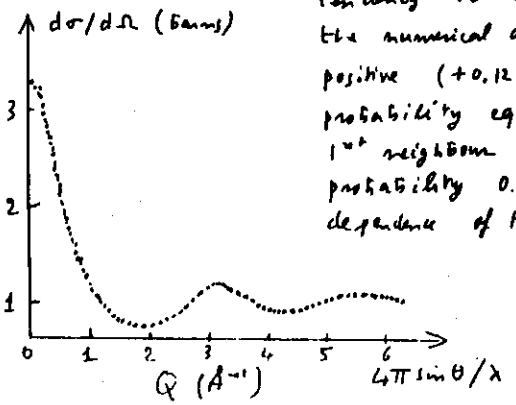

- Short-range order in Ni_3Fe [8, 20]

This has been studied on samples isotopically enriched with ^{62}Ni, quenched from above $T_c \simeq 500$ °C (LRO superstructure type Cu_3Au). The alloy shows no static displacements, and the d_{eenn} values deduced by Fourier transform of $(d\sigma/d\Omega)_{SRO}$ up to ≃ 40 neighbour shells.

The figure shows measured and reconstructed diffuse intensity maps, and the dependence of $\alpha(R_{eenn})$.

The signs of the α agree with those of the LRO Ni_3Fe superstructure ($\alpha_{eennodd} = -1/3$, $\alpha_{eenn\,even} = +1$), showing that the SRO and the LRO are of the same nature.

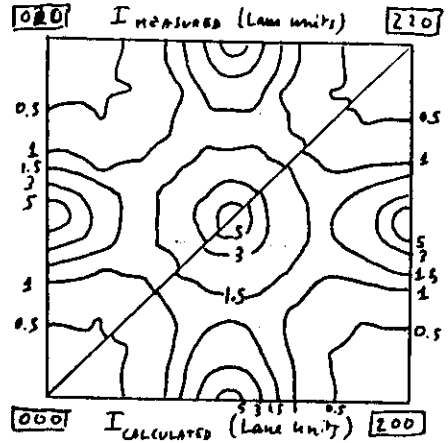

Ni_3Fe quenched from 507 °C
(001) reciprocal plane

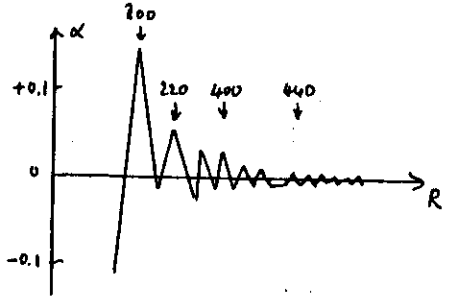

(d) Simulation of the crystal structure from the SRO parameters

The α's are of course not independent. Tentatives have been made to simulate the SRO crystal structure by computational methods, imposing the first α's (typically 4 to 6) to a box containing N 10 000 atoms ; one starts from differentiated initial states, exchange pairs of atoms until the final α converge to the imposed values [21]. The results of such calculations are still under discussion ; they seem to allow to deduce numbers of triplets (A-A-A, A-B-B, A-A-B, B-B-B) in quadruplets, but one should be more cautious with the analysis in terms of microdomains [22].

ⓔ Transition states and cluster models

In some compounds presenting substitutional disorder (carbides MC_{1-x}, TiO_x, $LiFeO_2$, $Ti_{1+x}S_2$, ...), the diffuse scattering in reciprocal space is practically restricted to surfaces or lines. This has been in particular observed by electron diffraction, and interpreted by several authors [23,24,25] in terms of cluster models, from a generalization of the Pauling rule (generally applied to ionic solids) which states that the small blocks of a structure have as much as possible a composition identical to that of the bulk compound. For example, for $NbC_{0.83}$ (see figure below), this suggests that each Nb is surrounded by octahedra composed of 5C and 1 vacancy, randomly oriented (this has been confirmed by N.M.R.). Nevertheless, X-ray or neutron scattering performed on such systems show that the surface has a "width", that the intensity is modulated along it, and therefore that the "transition state" interpretation is an (interesting) first approximation.

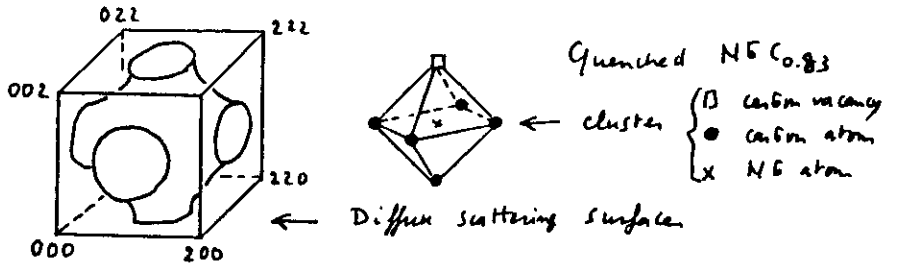

III. 4. Dilute Alloys: Atomic Displacements

Point defects in a metal (impurities, vacancies, self-interstitials) induce strain field in the lattice, which contains two contributions:

- an homogeneous expansion or contraction: $\vec{R_n} \longrightarrow \vec{R_n^a}$
- size effects. the atoms are no more exactly at the lattice positions $\vec{R_n^a}$, but displaced by $\vec{u_n} = \vec{x_n} - \vec{R_n^a}$.

ⓐ General formalism

We suppose that the concentration x in defects is small ($x \ll 1$), that the defects are random, non interacting, and that the diffuse scattering intensity will be Nx times that of an isolated defect situated at the origin. We assume superposition of the displacement fields of these Nx defects.

The elastic diffuse cross-section is then:

$$d\sigma/d\Omega)_{AD} \simeq Nx \left[b_0 + \sum_n b_A e^{i\vec{Q}.\vec{R_n}} \right]^2 \qquad \left(\begin{matrix} AD : \text{atomic} \\ \text{displacements} \end{matrix}\right)$$

b_A is the scattering length of the matrix atoms, b_0 that of the defect (b_0 for an interstitial B, $-b_A$ for a vacancy, $b_B - b_A$ for a substitutional impurity B).

If the displacements are small compared to interatomic distances ($|\vec{u_n}| \ll a$) and $\vec{Q}$ is in the first or second Brillouin zone, one can develop to first order in $\vec{u_n}$:

$$e^{i\vec{Q}.\vec{x_n}} \simeq (1 + i\,\vec{Q}.\vec{u_n})\, e^{i\vec{Q}.\vec{R_n}}, \quad \sum_n e^{i\vec{Q}.\vec{R_n}} = 0 \text{ outside the}$$

Bragg peaks, and one can show that the summation $\sum_n \vec{u_n} e^{i\vec{Q}.\vec{R_n}}$ converge to $\tilde{\vec{u}}(\vec{Q})$. Then:

$$d\sigma/d\Omega)_{AD} \simeq Nx \left[b_0 + i\, b_A\, \vec{Q}.\tilde{\vec{u}}(\vec{Q}) \right]^2$$

where $\tilde{\vec{u}}(\vec{Q})$ is the Fourier transform of the defect induced displacement field.

Contrary to $d\sigma/d\Omega)_{SAD}$, $d\sigma/d\Omega)_{AD}$ is not periodic in the reciprocal space.

In fact, the atomic displacements $\vec{u_n}$ are not independent, as there is bonding between all atoms: one introduces the KANZAKI forces [26]: these are virtual forces $\vec{f_n}$ which, applied to near neighbours $\vec{x_n}$ of the point defect, produce in its absence the same displacements.

In the harmonic approximation, with Born-von-Karman limit conditions, $\vec{f_n}$ and $\vec{u_m}$ are related by the Hooke's law: $\vec{f_n} + \overline{\overline{\Phi_{nm}}}\,\vec{u_m} = 0$, where $\overline{\overline{\Phi_{nm}}}$ is the force constant

matrix (static Green function) between atoms n and m, which can be obtained from the phonon spectrum.

The Fourier transforms of $\vec{f}$, $\overline{\overline{\Phi}}$ and $\vec{u}$ are related by

$$\tilde{\vec{f}}(\vec{Q}) + \tilde{\overline{\overline{\Phi}}}(\vec{Q}) . \tilde{\vec{u}}(\vec{Q}) = 0 \qquad (*)$$

Then: $d\sigma/d\Omega)_{AD} \simeq N x \left[b_0 + i b_A \vec{Q} . \tilde{\overline{\overline{\Phi}}}^{-1}(\vec{Q}) . \tilde{\vec{f}}(\vec{Q}) \right]^2$ /3/

which depends only on a small number of Kanzaki force parameters: one fits the experimental data with a reasonable set of $\vec{f_n}$, then calculates $\vec{u_m} = \overline{\overline{\Phi}}^{-1}_{nm} \vec{f_n}$.

- For anisotropic defects, one must of course average $d\sigma/d\Omega)_{AD}$ on all possible orientations of the defect,
- If the neighbour displacements are large (i.e. for interstitials) one must introduce a correction term in the scattering amplitude, and treat these displacements as free parameters).

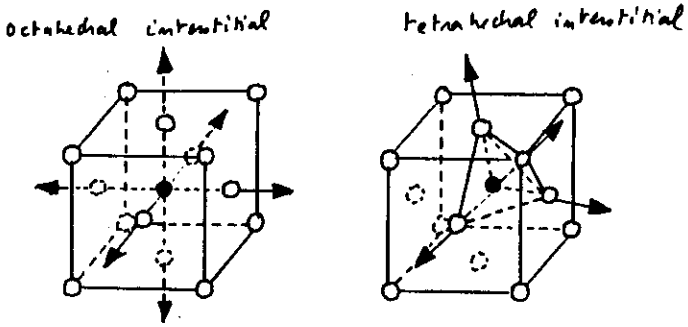

KANZAKI FORCES IN FCC CRYSTAL
(on first neighbours)

(*) $\tilde{\overline{\overline{\Phi}}}(\vec{Q})$ is defined by $\frac{1}{N} \sum_{nm} \overline{\overline{\Phi}}_{nm} e^{i\vec{Q}.(\vec{R_n} - \vec{R_m})}$; if $\vec{Q}$ is parallel to a symmetry axis of a cubic crystal,

$$\tilde{\overline{\overline{\Phi}}}(\vec{Q}) = m_A \begin{pmatrix} \omega_L^2(\vec{Q}) & 0 & 0 \\ 0 & \omega_{T_1}^2(\vec{Q}) & 0 \\ 0 & 0 & \omega_{T_2}^2(\vec{Q}) \end{pmatrix}$$

where ω_L, ω_{T_1}, ω_{T_2} are the phonon frequencies, and m_A the mass of a matrix atom.

Applications:

- BAUER [27] measured the elastic diffuse neutron scattering of neutrons by several aluminium dilute alloys, among which a Al – 0.8% Cu single crystal at 900°C (to avoid formation of Guinier-Preston zones); the experimental results are in good agreement with formula /3/, using radial Kanzaki forces on the two first neighbour shells: $f_1 = -4.2\ 10^{-10}$ N and $f_2 = -0.2 f_1$; this and the fact that when $\vec{Q} \to 0$, $d\sigma/d\Omega)_{AD}$ is larger than the Laue value, are in agreement with the observation that the Cu atoms contract the Al matrix (from $da/a dx$).

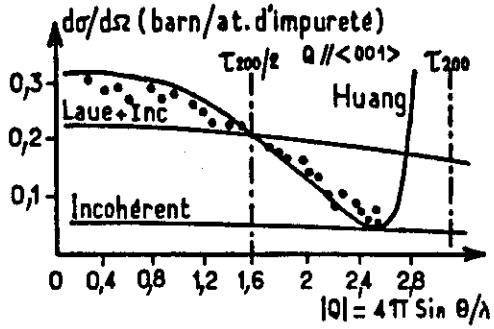

- By X-ray diffuse scattering at 4 K, HAUBOLD [4, 6] showed that the self-interstitial structure in most fcc crystals (introduced by electron irradiation) is a split dumbbell.

(b) Huang scattering

Let's look near the Bragg peak $\vec{\tau}_{hkl}$ and define $\vec{q} = \vec{Q} - \vec{\tau}_{hkl}$ ($|\vec{q}| << \pi/a$). $\tilde{\vec{u}}(\vec{Q})$, $\tilde{\vec{f}}(\vec{Q})$ and $\tilde{\overline{\overline{\Phi}}}(\vec{Q})$ are periodic in the reciprocal space, and depend only on $\vec{q}$. At small $\vec{q}$, $\omega(\vec{q})$ is proportional to q and $\tilde{\overline{\overline{\Phi}}}^{-1}(\vec{q}) = q^{-2} \tilde{\overline{\overline{\Phi}}}^{-1}(\vec{e_q})$, where $\vec{e_q}$ is the unitary vector in direction $\vec{q}$. On the other hand, $\tilde{\vec{f}}(\vec{Q}) = \sum_n \vec{f_n} e^{i\vec{q}.\vec{R_n}} \simeq \sum_n \vec{f_n} (i\vec{q}.\vec{R_n})$ because $\sum_n \vec{f_n} = 0$ (a defect does not deplace the crystal as a whole).

One introduces the dipolar elastic tensor of the defect, $\overline{\overline{P}}$,

such that $P_{ij} = \sum_n f_n^i R_{nj}$. Therefore $\tilde{J}(\vec{q}) \simeq i q \, \bar{\bar{P}} \, \vec{e}_q$.

When $\vec{q} \to 0$, the second term of the scattering amplitude diverges as $1/q$, and the intensity as $1/q^2$: this is the Huang scattering: $\left(d\sigma/d\Omega\right)_{A0}^{\vec{q}\to 0} \simeq \left(d\sigma/d\Omega\right)_{Huang} \simeq N x b_0^2 q^{-2} \left[\vec{\tau}_{hkl} \cdot \bar{\bar{\Phi}}^{-1}(\vec{e}_q) \, \bar{\bar{P}} \, \vec{e}_q^{\,0}\right]^2$

Physically, the symmetry of the dipole tensor $\bar{\bar{P}}$ is intimately related to that of the distortion introduced by the defect, and the site of the point defect can be deduced from the symmetry of the Huang scattering around the Bragg reflexions.

For an isotropic impurity in a cubic lattice:

$$\left(d\sigma/d\Omega\right)_{Huang} = N x \, b_A^2 \, q^{-2} \, \frac{\left(C_{11}+2C_{12}\right)^2}{m_A^2 \, V_{hkl}^2} \left(\frac{da}{a\,dx}\right)^2 \left(\vec{\tau}_{hkl} \cdot \vec{e}_q\right)^2$$

(V_{hkl} longitudinal speed of sound, C_{11}, C_{12}, elastic constants).

The Huang scattering shows nodal planes defined by $\vec{\tau}_{hkl} \cdot \vec{q} = 0$, i.e. $\vec{q} \perp \vec{\tau}_{hkl}$, where the intensity equals zero.

If the impurity is anisotropic, one must average on its possible orientations, and the nodal planes may reduce to a nodal line or vanish.

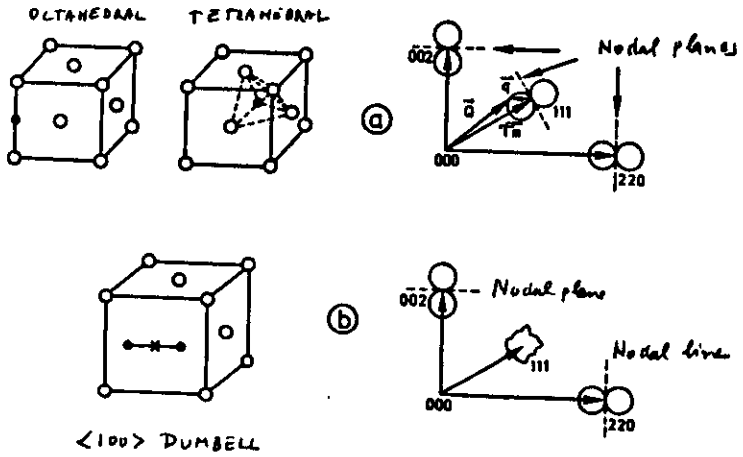

Contours of the Huang scattering for point defects (interstitials) in f.c.c. crystal.

Huang scattering increases with the strain field of the point defect $(da/a\,dx)^2$: it is much larger for interstitials than for vacancies; the q^{-2} variation is directly related to the R^{-2} dependence of the point defect strain field at large distance R.

In the case of defect clusters containing N_a point defects each, with additivity of the defect strain field, $\left(d\sigma/d\Omega\right)_{Huang}^{cluster}$ will be proportional to $\frac{Nx}{N_a}\left(N_a \frac{da}{a\,dx}\right)^2 = N_a \, N x \left(\frac{da}{a\,dx}\right)^2$: it will be equal to N_a times the Huang scattering of the Nx point defects randomly distributed. This shows that, in any case, qualitatively the clustering of point defects increases strongly the Huang scattering; but the $\vec{q}$ domain where the Huang approximation is valid ($d\sigma/d\Omega \propto q^{-2}$) becomes narrower.

Applications

EHRHART and SCHILLING [7] have measured at 4 K the Huang scattering of electron irradiated Al single crystals containing 5.10^{-4} Frenkel pairs. Around the (400) Bragg reflexion, the diffuse intensity after irradiation remains unchanged in the <011> direction, but increases strongly along <100>: this increase varies as q^{-2}. There is in first approximation a nodal plane where the Huang scattering is zero, which allowed the authors to eliminate the <111> and <110> dumbbell structures for the self-interstitial (But the true solution: <100> dumbbell rather than octahedral or tetrahedral interstitial was only found after measurements far from the Bragg peaks [4,6]).

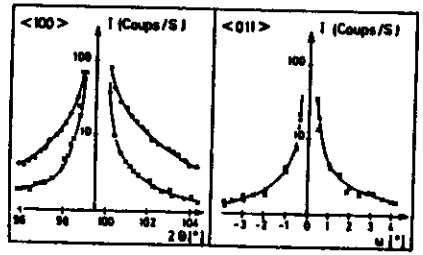

Huang scattering of irradiated Al.
(400) Bragg reflexion
x: before irradiation
o: after irradiation

After isochronal anneals, the Huang scattering in Al increases rapidly between 40 and 150 K, then decreases and vanishes around 300 K: this is associated to the formation and dissolution of interstitial vacancy loops [7].

Electron irradiated Al

——— electrical resistivity
..... (400) and (200) Bragg peaks in the <011> direction (nodal plane at 4 K)
-.-.-.- (400) and (200) Bragg peaks in the <100> direction

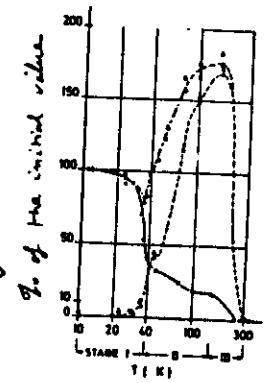

More recently, the precise scattering near the Bragg peaks due to vacancy and interstitial loops has been calculated and shown to differ [28,29]; in the figure → the size distribution of loops in irradiated copper (with 60 MeV Ni^{+}) is compared to that obtained from transmission electron microscopy; the latter found an excess of interstitial loops; much more small loops in the range 10 - 30 Å are deduced from the Huang diffuse, which give an equal concentration of vacancies and interstitials [28]

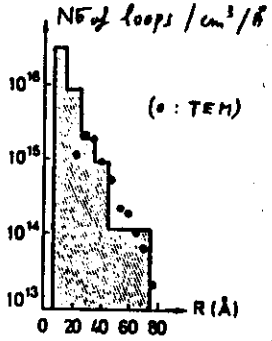

III. 5. Concentrated alloys: separation of the order and displacement terms

This separation can be made if the static displacements are not too important ($\lesssim 0.1$ Å). The method, due mainly to SPARKS and BORIE [30] and developped by HAYAKAWA et al [31], WILLIAMS [32] and TIBBALS [33], allows to obtain the SRO coefficients α and information on the relative atomic displacements $\vec{u}_{ij} = \vec{u}_i - \vec{u}_j$ by a 2nd order development of $e^{i\vec{Q}\cdot\vec{u}_{ij}}$ $\left(\simeq 1 + i\vec{Q}\cdot\vec{u}_{ij} - \frac{1}{2}(\vec{Q}\cdot\vec{u}_{ij})^2\right)$

$$\frac{d\sigma}{d\Omega}(\vec{Q}) = \sum_{i,j}^{N} b_i b_j \, e^{i\vec{Q}\cdot(\vec{R}_i - \vec{R}_j)} \, e^{i\vec{Q}\cdot\vec{u}_{ij}}$$

and by a comparison of the intensities measured in various reciprocal lattice cells. We shall not detail this method here. Schematically, $d\sigma/d\Omega$ is written under the form:

$$\frac{d\sigma}{d\Omega} = \left(\frac{d\sigma}{d\Omega}\right)_{SRO} + N x(1-x)\left[h_1 P_x(h_1,h_2,h_3) + h_2 P_y + h_3 P_z + h_1^2 R_x(h_1,h_2,h_3) + h_2^2 R_y + h_3^2 R_z + h_1 h_2 S_{xy}(h_3,h_1,h_3) + h_2 h_3 S_{yz} + h_3 h_1 S_{zx}\right]$$

where $(d\sigma/d\Omega)_{SRO}$ does not depend of displacements and is given by formula /1/ of § III.3 ; P_x, R_x, S_{xy} are periodic in the reciprocal space and depend linearly respectively of the relative atomic displacements (i.e. P_x to $\overline{u^{x,AB}_{lmn}}$, ...) and mean square relative atomic displacements (R_x to $\overline{(u^{x,AB}_{lmn})^2}$ and S_{xy} to $\overline{u^{x,AB}_{lmn}\, u^{y,AB}_{lmn}}$, ...).

The importance of the 3 terms in $d\sigma/d\Omega$ (i.e. $d\sigma/d\Omega)_{SRO}$, the linear term and the quadratic term in h_i, $i = 1,2,3$) is given below for Cu_3Au quenched from 500° C [34]:

A: measured curve (——)
B: modulation due to size effect (P_x, P_y, P_z) (.....)
C: measured curve corrected for size effect (difference A - B : - - - -)
D: second order term (-.-.-.-)

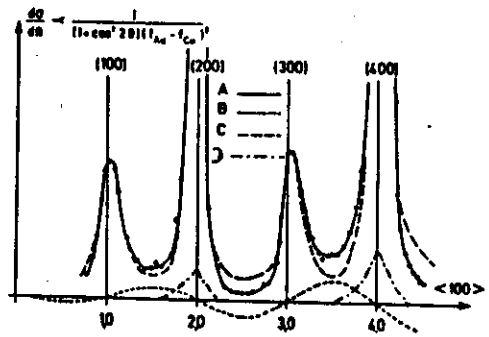

By linear combination of the measurements in different cells of the reciprocal space, a mean-square fit, one can deduce $(d\sigma/d\Omega)_{SRO}$, P_x, R_x, S_{xy}, and by Fourier transform the u_{lmn} and linear combinations of the $\overline{u_{lmn}}$ and of the $\overline{(u_{lmn})^2}$.

Applications

- The Sparks and Borie method was first applied to 2nd nickel to $Cu\,Al_{0.15}$ [35,36]. The average static displacement deduced is $\simeq 0.01$ Å and the proposed local order suggests that 1st Al-Al neighbour pairs are practically forbidden.

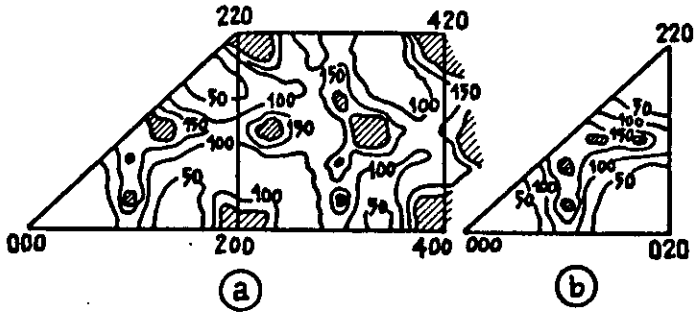

Measured — After 1st order Sparks & Borie correction

- The $Ti\,N_{0.82}$ system was studied by in-situ neutron diffuse scattering at 700, 800 and 900 °C; an average contraction of 0.01 Å of the first neighbour Ti–N distance is observed; the diffuse intensity due to SRO of nitrogen vacancies is maximum in ½ ½ ½ ($\alpha_1 = -0.09$, $\alpha_2 = -0.10$, $\alpha_3 = +0.04$, $\alpha_4 = +0.015$ at 800 °C) and the effective pair potentials deduced from this experiment were given in § III.3 [15,37]. The metal-metalloid first neighbour contraction is even stronger ($\simeq 0.03$ Å) in the carbide $Ti\,C_{0.74}$ and $NbC_{0.73}$ [38].

- The ternary austenite $Fe_{0.56}\,Cr_{0.21}\,Ni_{0.23}$ was studied by diffuse neutron scattering, using different isotopic enrichments:
  sample 1: natural Fe ($b = 0.954\ 10^{-12}$ cm), ^{62}Ni ($b = -0.83$), ^{52}Cr ($b = 0.488$)
  sample 2: ^{54}Fe ($b = 0.42$), ^{62}Ni, ^{52}Cr
  sample 3: natural Fe, ^{58}Ni ($b = 1.437$), ^{52}Cr.
  This allowed to obtain separately the 3 families of SRO coefficients: $\alpha_{1\,0\,0}^{Fe\text{-}Cr}$, $\alpha_{1\,0\,0}^{Fe\text{-}Ni}$, $\alpha_{1\,0\,0}^{Ni\text{-}Cr}$ and to show a weak tendency to segregation for Ni–Fe, and a weak tendency to order for Fe–Cr (in 1½0) and Ni–Cr (in 100 and 110) [39].

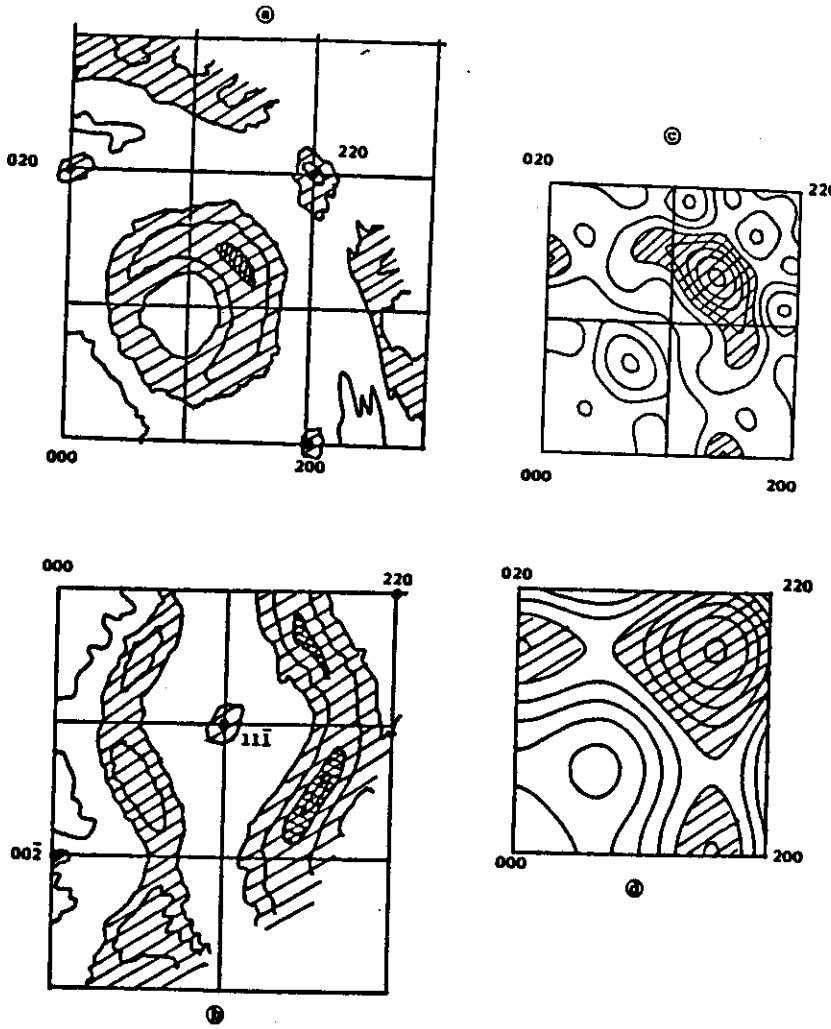

Elastic neutron diffuse scattering maps in $Ti\,N_{0.82}$.
(a) (001) reciprocal plane (b) (1T0) reciprocal plane
(c) Separated 1st order displacement contribution
(d) Calculated 1st order displacement contribution assuming a shortening of Ti–N 1st neighbour distance only.
(T. PAIEW, B. BEUNEU, C.H. de NOVION).

III. 6 Small-angle scattering

This is diffuse scattering around the direct beam, at small scattering vector, namely $10^{-3}\ \text{Å}^{-1} \lesssim |\vec{Q}| = 4\pi\theta/\lambda \lesssim 0.2\ \text{Å}^{-1}$ ($|\vec{Q}|$ is smaller than the smallest reciprocal lattice vector). It allows to study variations of scattering length densities (i.e. inhomogeneities, precipitation, ...) in the range 10 – 1000 Å, when the atomic arrangement of an alloy can be replaced by a continuous variation of scattering length densities.

(a) General formalism (summary)

One defines the scattering length density $\rho(\vec{x}) = \overline{\frac{b}{\Omega}}$ (Ω = atomic volume, $\overline{b}$ averaged on a volume d^3x small, but large compared to Ω). $\overline{b}$ and Ω depend in principle of $\vec{x}$.

The differential scattering cross-section becomes:

$$\left(\frac{d\sigma}{d\Omega}\right)_{SAS}(\vec{Q}) = \left| \int_V \rho(\vec{x}) \exp(i\vec{Q}.\vec{x})\, d^3\vec{x} \right|^2 \qquad (V = \text{sample volume})$$

The integrated intensity obeys to the general relationship:

$$\int \left(\frac{d\sigma}{d\Omega}\right)_{SAS}(\vec{Q})\, d^3\vec{Q} = N V (2\pi)^3 \overline{[\rho(\vec{x}) - \overline{\rho}]^2},$$ mean-square fluctuations of scattering length density.

Two-phase model

One assumes particles embedded in a matrix of homogeneous scattering length density ρ_M, with sharp interface. ρ_p is the scattering length density of the particle. One has then:

$$\left(\frac{d\sigma}{d\Omega}\right)_{SAS}(\vec{Q}) = (\rho_p - \rho_M)^2 \left| \int_{\substack{\text{Total volume} \\ \text{of particles}}} \exp(i\vec{Q}.\vec{x})\, d^3x \right|^2$$

One defines the particle form factor: $F_p(\vec{Q}) = \frac{1}{V_p}\int_{V_p} \exp(i\vec{Q}\vec{x})\, d^3\vec{x}$, where the origin is taken at the centre of gravity of the particle.

For N_p particles of volume V_p, indexed by i, j:

$$\frac{1}{V_p^2}\left| \sum_i \int_{V_p} \exp(i\vec{Q}.\vec{x})\, d^3\vec{x} \right|^2 = N_p |F_p(\vec{Q})|^2 + \sum_{i \neq j} e^{i\vec{Q}(\vec{R}_i - \vec{R}_j)} F_i(\vec{Q}) F_j(\vec{Q})$$

and

$$\left(\frac{d\sigma}{d\Omega}\right)_{SAS}(\vec{Q}) = (\rho_p - \rho_M)^2 N_p V_p^2 |F_p(\vec{Q})|^2 \left[1 + \psi(\vec{Q})\right]$$

$\psi(\vec{Q})$ is an interference term equal to $\frac{1}{N_p}\sum_{i \neq j} e^{i\vec{Q}(\vec{R}_i - \vec{R}_j)}$

- $= 0$ if the particles are dilute and at random,
- $\neq 0$ if the concentration of particles is large (correlations for a hard sphere model for example).

For spheres of radius R_s, $|F_p(\vec{Q})|^2 = \dfrac{3\sin(QR_s) - QR_s\cos(QR_s)}{Q^3 R_s^3}$

For identical hard spheres in total concentration $c_p = N_p V_p / V$, the functions $|F_p(\vec{Q})|^2$, $1 + \psi(\vec{Q})$ and $d\sigma/d\Omega)_{SAS} \propto |F_p(\vec{Q})|^2[1 + \psi(\vec{Q})]$ have the following shape:

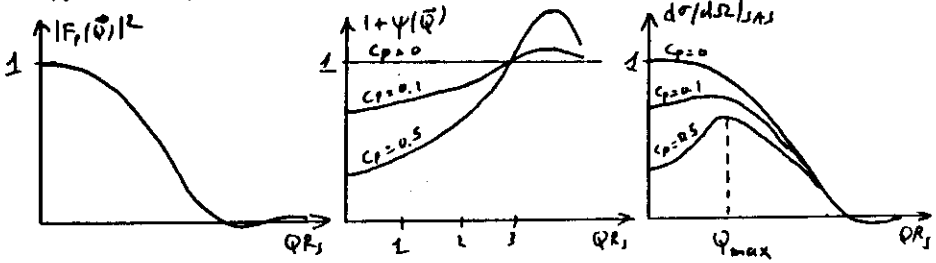

- In the dilute case, $d\sigma/d\Omega)_{SAS}$ is a decreasing function of $|\vec{Q}|$.
- In the concentrated case, particles are short-range-ordered, and $d\sigma/d\Omega)_{SAS}$ shows a maximum at $Q = Q_{max} \simeq 1/d$, inverse average distance of near neighbour particles; for $Q > Q_{max}$, the cross-section converges with the independent particle curve.

Three general relations can be recalled in the non-interacting case:

- When $\vec{Q} \to 0$, $d\sigma/d\Omega\ (\vec{Q} \to 0) \to N_p V_p^2 (\rho_p - \rho_M)^2$ (as $|F_p(0)|^2 = 1$)
- POROD approximation: at large $|Q|$ (>> (particle dimensions)$^{-1}$), $|F(\vec{Q})|^2 \simeq 2\pi N A_p / V_p^2 Q^4$: the scattering cross-section varies as Q^{-4} and is related to the interface area A_p.

- GUINIER approximation : at small $|Q|$ ($\ll 1/a$, a characteristic dimensions of the particle), $|F(\vec{Q})|^2 \simeq \exp(-Q^2 R_D^2/)$, where R_D^2 is the gyration radius of the particle in direction D :

$$R_D^2 = \frac{1}{V_p}\int r_D^2 A_{r_D}\, dr_D \quad , \quad D \perp \vec{k_0} \quad , \quad A_{r_D} \text{ cross-section area of the particle along the line } r_D$$

(with the origin chosen at the center of gravity of the particle).

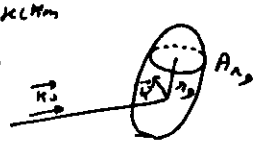

For randomly oriented particles, $|F(\vec{Q})|^2 = \exp(-Q^2 R_G^2/3)$,

$$R_G^2 = \frac{1}{V_p}\int_{V_p} r^2\, d^3r \qquad (\text{for a sphere, } R_G = \sqrt{3/5}\, R_S).$$

Remarks :

- The equations have been extended (at least in the non-interacting case) for size distribution of particles
- Small-angle scattering can occur with continuous variation of scattering density $\rho(\vec{r})$ (no interface) :
  - Composition fluctuations (spinodal decomposition),
  - critical scattering (near order-disorder phase transitions),
  - dislocations (due to the change of scattering density at the core of edge dislocations).
- There is a magnetic contribution to neutron SAS in ferromagnetic substances

(b) Experimental details

Small-angle scattering has a much more intense signal than large-angle diffuse scattering : with neutrons, samples of thickness 0.1 mm (surface $\simeq 1\,cm^2$) have been studied [44]. Large wavelengths are preferred in order to avoid multiple Bragg scattering (cold neutrons, synchrotron radiation) ; one or two (bi-dimensional) position sensitive detectors are currently used.

With neutrons, the spectrometer is often at the extremity of a guide tube, and the beam monochromatized by a mechanical velocity selector ; changing the sample-detector distance allows to optimize the range of Q studied.

The data are fitted by analytical or numerical methods ; in the first case, it is necessary to extrapolate $d\sigma/d\Omega_{SAS}$ at $\vec{Q}=0$ and $\vec{Q}=\infty$ (generally by using the Guinier and Porod laws respectively, but this is not always possible, and very careful measurements are needed) ; in the second case, one uses various functions to describe the particle distribution (log normal functions, Pearson functions, etc....).

Preliminary transmission electron microscope study is essential to suggest the type of model to be used (shape of particles, one or several types of particles, etc....).

(c) Examples

- Small-angle scattering has been largely used for the study of precipitation after aging of Al-based alloys (Al-Zn, Al-Mg, ...) (Kinetics of phase separation, growth of Guinier-Preston zones, etc...).

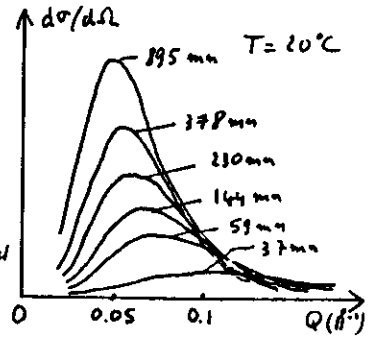

The neutron SAS study Al - 5.3 at% Zn, quenched from above the miscibility gap and aged at 20°C showed that the scattering is isotropic at large $|Q|$ at short ageing times, and became anisotropic at longer times : phase separation leads to spherical G.P. zones, which subsequently transform in ellipsoids of axis <111>. The $|Q|$ averaged scattering for various ageing times is shown on the above figure. $Q^3\, d\sigma/d\Omega(Q)$ scales to a unique curve as predicted by Monte-Carlo simulations using a 3-dimensional Ising model - Two different kinetic behaviours are obtained at 20 and 110°C.

- Neutron SAS has been used to characterize the distribution of precipitates in alloys, and its evolution with aging at different times and temperatures : $Ni_3(Al,Ti)$ γ' phase in high nickel content austenitic steels [41, 42], $M_{23}C_6$ carbide in stainless steels [43].

In the latter case ($Fe_{0.70}Cr_{0.18}Ni_{0.10}$ + 0.069 % weight C), the volume concentration of carbides is as low as 5.10^{-3}. The particles are relatively isotropic and their size distribution obtained with a good precision. → A bimodal distribution is suggested, with intragranular and (larger) grain-boundary precipitates [43].

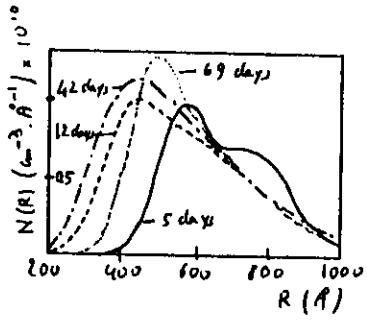

- The use of isotopic substitution has led to very interesting results in the case of He bubbles in α-particle irradiated nickel [44, 45]. In this experiment, the contrast in scattering length density can be written: $\Delta\rho = \frac{b_{Ni}}{\Omega_{Ni}} - \frac{b_{He}}{\Omega_{He}}$, where Ω_{Ni} and Ω_{He} are the atomic volumes of Ni and He; the pressure of He in the bubbles, and therefore Ω_{He}, is not known (it is only indirectly derived from the size, assuming pressure is balanced by surface tension). The idea was to derive Ω_{He} from the ratio of two experiments using respectively Ni^{58} ($b = 1.44\ 10^{-12}$ cm) and Ni^{60} ($b = 0.28\ 10^{-12}$ cm) matrix. Of course, one has to take into account a size distribution of the bubbles, the pressure in the bubbles changing with the size. The analysis of $d\sigma/d\Omega$ in Ni^{58} gave a bimodal distribution, with a set of bubbles of size $\simeq 10$ Å, dominating $d\sigma/d\Omega$ around 0.1 $Å^{-1}$, and a set of size $\simeq 100$ Å, dominating the scattering around 0.02 $Å^{-1}$. The quasi-extinction of the 10 Å bubble contribution in ^{60}Ni showed that the mean He atomic density is 0.7 of atomic Ni density. The large bubbles were observed by TEM only after the SAS experiment, and found localized mostly near the surface; the He atomic density in the large bubbles is weak (< 1/7 Ni atomic density).

- Another new development is the use of anomalous x-ray small angle scattering for the study of ternary alloys [46,47]. This was done recently to study the composition change during ageing of Al Zn Ag alloys. In such a system, with 2 phases (rich Al matrix, and Zn-Ag enriched G.P. zones), it can be shown that:
$d\sigma/d\Omega)_{SAS} \propto (\Delta C_{Zn} F_{Zn}(E) + \Delta C_{Ag} F_{Ag})^2 |F_p(\vec{Q})|^2$,
where ΔC_{Zn} and ΔC_{Ag} are the concentration differences in Zn and Ag between precipitate and matrix, $F_i = f_i - f_{Al}$, and E = energy of the incident synchrotron radiation.
Increasing E near the K-absorption edge of Zn decreases f_{Zn} (see § I.3) and the contrast between precipitate and matrix.

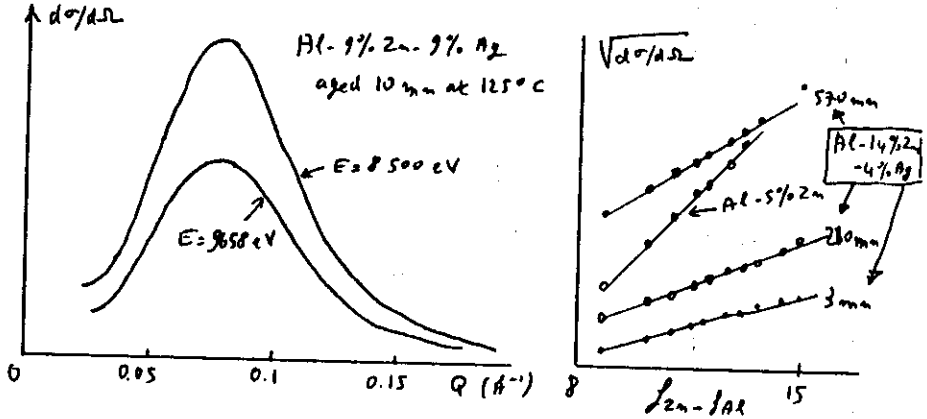

A linear relation is shown between $\sqrt{d\sigma/d\Omega}$ and $F_{Zn}(E)$: from this, $\Delta C_{Zn}/\Delta C_{Ag}$ is calculated. It was shown that during anneals around 125 °C, the ratio $\Delta C_{Zn}/\Delta C_{Ag}$ remained constant in Al-9 at% Zn-9 at% Ag, while it decreased from 0.47 to 0.27 in Al-14 at% Zn-4 at% Ag, when particles transform from Guinier-Preston zones to E' coherent precipitates [47]

REFERENCES

[1] A. GUINIER, R. GRIFFOUL, C. R. Acad. Sc. Paris 221 (1945) 555, Revue de Métallurgie XLV (1948) 387

[2] J.M. COWLEY, J. Appl. Phys. 21 (1950) 24.

[3] J.P. POUGET, "Solid State Phase Transformations in Metals and Alloys", Les Editions de Physique, Orsay, France (1980) p. 253.

[4] P. EHRHART, H.G. HAUBOLD, W. SCHILLING, Adv. in Solid State Physics 14 (1974) 87.

[5] M. BESSIERE, S. LEFEBVRE, Y. CALVAYRAC, F. BLEY, M. FAYARD, J. Appl. Cryst. 15 (1982) 94.

[6] H.G. HAUBOLD, Rev. Physique Appliquée (Paris) 11 (1976) 73.

[7] P. EHRHART, W. SCHILLING, Phys. Rev. B8 (1973) 2604

[8] S. LEFEBVRE, F. BLEY, M. BESSIERE, M. FAYARD, H. ROTH, J.B. COHEN, Acta Cryst. A36 (1980) 1.

[9] C.H. de NOVION, W. JUST, J. Phys. F: Metal Phys. 8 (1978) 1627

[10] M.A. KRIVOGLAZ, "Theory of X-Ray and Thermal Neutron Scattering by Real Crystals", Plenum Press, New-York (1969)

[11] P.C. CLAPP, S.C. MOSS, Phys. Rev. 142 (1966) 418 and 171 (1968) 754
S.C. MOSS, P.C. CLAPP, Phys. Rev 171 (1968) 764.

[12] M. BESSIERE, S. LEFEBVRE, Y. CALVAYRAC, Acta Cryst. B39 (1983) 145.

[13] R.A. TAHIR-KHELI, Phys. Rev. 188 (1969) 1142

[14] H.M. GILDER, S. VIGNESOULT, J. Phys. F: Metal Phys. 14 (1984) 1795

[15] T. PRIEM, B. BEUNEU, C.H. de NOVION, F. LIVET, to be published

[16] R. KIKUCHI, Phys. Rev. 81 (1951) 988 and J. Phys. Colloq 38 (1977) C7-307

[17] S.C. MOSS, Phys. Rev. Lett. 22 (1969) 1108

[18] J.R. CASTLES, J.M. COWLEY, A.E.C. SPARGO, Acta Cryst. A27 (1971) 376.

[19] J. VRIJEN, S. RADELAAR, Phys. Rev. B17 (1978) 409.

[20] S. LEFEBVRE, F. BLEY, M. FAYARD, M. ROTH, Acta Met. 29 (1981) 749

[21] P. GEHLEN, J.B. COHEN, Phys. Rev. 139 (1965) A 844

[22] F. BLEY, P. CONEDESE, S. LEFEBVRE, in "Phase Transformations in Solids", ed. Tsakalakos, North-Holland (1984).

[23] M. BRUNEL, P. de BERGEVIN et al, J. Phys. Chem. Solids 30 (1969) 2011 and 33 (1972) 1927

[24] M. SAUVAGE, E. PARTHE, Acta Cryst. A28 (1972) 607 and A30 (1974) 239

[25] R. de RIDDER, G. VAN TENDELOO, D. VAN DYCK, S. AMELINCKX, Phys. Stat. Sol (a) 38 (1976) 663, 40 (1977) 669, 43 (1977) 541

[26] H.J. KANZAKI, J. Phys. Chem. Solids 2 (1957) 24.

[27] G.S. BAUGA, Report KFA-Jülich, JÜL-1158 (1975)

[28] B.C. LARSON, F.W. YOUNG Jr, in "Point Defects and Defect Interaction in Metals", Univ. of Tokyo Press, Tokyo (1982) p. 679

[29] P. EHRHART, B. SCHÖNFELD, K. SONNENBERG, id [28] p. 687.

[30] C.J. SPARKS, B. BORIE, in "Local Arrangements studied by X-ray diffraction", Gordon and Breach, New York (1966) p. 5.
B. BORIE, C.J. SPARKS, Acta Cryst. A27 (1971) 198.

[31] M. HAYAKAWA, P. BARDHAN, J.B. COHEN, J. Appl. Cryst. 8 (1975) 87

[32] R.O. WILLIAMS, Report ORNL-4828 (1972), Oak Ridge National Laboratory, Tennessee (USA).

[33] J.E. TIBBALS, J. Appl. Cryst. 8 (1975) 111.

[34] B.E. WARREN, B.L. AVERBACH, B.W. ROBERTS, J. Appl. Phys. 22 (1951) 1493.

[35] B. BORIE, C.J. SPARKS, Acta Cryst. 17 (1964) 827

[36] J.E. EPPERSON, I. FÜRNROHR, C. ORTIZ, Acta Cryst. A34 (1978) 667.

[37] T. PAIEM, B. BEUNEU, C.H. de NOVION, R. CAUDRON, E. SOLAL, A.N. CHRISTENSEN, Solid State Communications (1987), in press.

[38] V. MOISY-MAURICE, C.H. de NOVION, A.N. CHRISTENSEN, W. JUST, Solid State Commun. 39 (1981) 661.

[39] P. CENEDESE, F. BLEY, S. LEFEBVRE, Acta Cryst. A40 (1984) 228

[40] P. GUYOT, in "Utilisation des faisceaux de neutrons en métallurgie", ed. J. Joffrin, Commissariat à l'Energie Atomique, Saclay, France (1985) P. 383.

[41] R. COPPOLA, S. RE FIORENTIN, Physica 136 B (1986) 465

[42] P. PIZZI, id ref. [40], P. 281.

[43] A. BOEUF, R.G.M. CACIUFFO, R. COPPOLA et al, J. Nucl. Mater. 126 (1984) 276

[44] D. SCHWAHN, H. ULLMAIER, J. SCHELTEN, W. KESTERNICH, Acta Metall. 31 (1983) 2003

[45] W. KESTERNICH, D. SCHWAHN, H. ULLMAIER, Scripta Met. 18 (1984) 1011

[46] O. LYON, J.J. HOYT, R. PRO et al, J. Appl. Crystallogr. 18 (1985) 480

[47] O. LYON, J.P. SIMON, Acta Met. 34 (1986) 1197.